https://doi.org/10.5194/hess-2022-187
Preprint. Discussion started: 28 June 2022

Hydrology and Earth System Sciences
Open Access
Discussions

Enhanced Watershed Modeling by Incorporating Remotely Sensed Evapotranspiration and Leaf Area Index

Sangchul Lee [a*], Dongho Kim [a], Gregory W. McCarty [b], Martha Anderson [b], Feng Gao [b], Fangni Lei [b], Glenn E. Moglen [b], Xuesong Zhang [b], Haw Yen [c], Junyu Qi [d], Wade Crow [b], In-Young Yeo [e], Liang Sun [f]

[a] School of Environmental Engineering, University of Seoul, Dongdaemun-gu, Seoul 02504, Republic of Korea

[b] USDA-ARS, Hydrology and Remote Sensing Laboratory, Beltsville, MD 20705, USA

[c] Crop Science, Bayer U.S., 700 W Chesterfield Pkwy W, Chesterfield, MO 63017, USA

[d] Earth System Science Interdisciplinary Center, University of Maryland, College Park, 5825 University Research Ct, College Park, MD 20740, USA

[e] School of Engineering, the University of Newcastle, Callaghan NSW 2308, Australia

[f] Key Laboratory of Agricultural Remote Sensing, Ministry of Agriculture / Institute of 14 Agricultural Resources and Regional Planning, Chinese Academy of Agricultural Sciences, 15 Beijing 100081, China

*** Corresponding author: Sangchul Lee (Sangchul.lee84@gmail.com or slee2020@uos.ac.kr)**

https://doi.org/10.5194/hess-2022-187
Preprint. Discussion started: 28 June 2022

Hydrology and Earth System Sciences Discussions

Abstract

To improve the capacity of watershed modeling, remotely sensed products are frequently used to reduce the uncertainty resulting from data limitations. Although remotely sensed evapotranspiration (RS-ET) products are widely used, vegetation parameters governing spatial and temporal variations in evapotranspiration (ET) are often not constrained by benchmark data. Recently, remotely sensed leaf area index (RS-LAI) products are becoming increasingly available, providing an opportunity to assess and improve simulated vegetation dynamics. The objective of this study is to assess the role of the two remotely sensed products (i.e., RS-ET and RS-LAI) in improving the accuracy of watershed model predictions. Specifically, we investigated the role of RS-ET and RS-LAI products in 1) reducing parameter uncertainty and 2) improving model capacity to predict the spatial distribution of ET and LAI at the sub-watershed level. The watershed-level assessment of the degree of equifinality (denoted as the number of parameter sets that produce equally acceptable model simulations) shows that less than half of the acceptable parameter sets for two constraints (streamflow and RS-ET; 14 parameter sets) are acceptable for three constraints (streamflow, RS-ET, and RS-LAI; six parameter sets). Among those six parameter sets, only three can satisfactorily characterize spatial patterns of ET and LAI at the sub-watershed level. Our results suggest that the use of multiple remotely sensed datasets holds great potential to reduce parameter uncertainty and increase the credibility of watershed modeling, particularly for characterizing spatial variability of hydrologic fluxes that are relevant to agricultural management.

Keywords: Remotely sensed evapotranspiration (RS-ET); remotely sensed leaf area index (RS-LAI); Soil and Water Assessment Tool (SWAT); predictive uncertainty

https://doi.org/10.5194/hess-2022-187
Preprint. Discussion started: 28 June 2022

Hydrology and Earth System Sciences
Discussions

1. Introduction

One major concern with regard to any hydrological modeling exercise is predictive uncertainty. Although the reliability of the simulated outcomes is assessed via model calibration and validation to some degree, predictive uncertainty always exists (Arnold et al., 2012; Yen et al., 2014a). The lack of observations is one of the primary sources of uncertainty. Majority of hydrological modeling studies depend solely on water quantity and/or quality measurements collected at watershed outlets (Arnold et al., 2012; Gassman et al., 2014). To overcome predictive uncertainty resulting from data shortfalls, the use of soft data (e.g., expert knowledge, literature, remotely sensed data, and extensive field monitoring) has been suggested as an additional constraint (Arnold et al., 2015; Lee et al., 2019; Seibert and McDonnell, 2002; Yen et al., 2016). Soft data have been used to better represent intra-watershed processes, that is hydrological processes that occur between streams and upland areas (Yen et al., 2014a). The inclusion of soft data has been found to be efficient in constraining model parameter values, leading to a reduction in predictive uncertainty (Julich et al., 2012; Lee et al., 2019; Vaché and McDonnell, 2006).

The Soil and Water Assessment Tool (SWAT) is a semi-distributed hydrological model that commonly encounters predictive uncertainty owing to a lack of observations (Gassman et al., 2014). One way to address this problem is to employ remotely sensed data into SWAT simulations to capture plant growth (Strauch and Volk, 2013; Yeo et al., 2014), wetland inundation dynamics (Lee et al., 2019; Yeo et al., 2019), and soil moisture (Chen et al., 2011). Compared to in-situ measurements that require intensive labor and high cost, remotely sensed data have the advantage of providing measurements across landscapes for a long period and reduce the problem of data deficiency for hydrologic model operations (Jiang and Wang, 2019; Xu et al., 2014). SWAT has been recently calibrated against remotely sensed evapotranspiration (RS-ET) products, leading to

https://doi.org/10.5194/hess-2022-187
Preprint. Discussion started: 28 June 2022

improved model predictions (Herman et al., 2018; Parajuli et al., 2018; Rajib et al., 2018; Wambura et al., 2018). Evapotranspiration (ET) is defined as the sum of evaporation and transpiration fluxes. It plays a critical role in water and energy cycling by transferring soil moisture to the atmosphere (Schlesinger and Jasechko, 2014). ET has been known as one of the largest fluxes of the components of water balance (Ukkola and Prentice, 2013). Thus, improved ET predictions can increase the overall accuracy of the model outcomes.

RS-ET products are commonly used as calibration data with streamflow to better constrain hydrologic parameters (Herman et al., 2018; Parajuli et al., 2018; Rajib et al., 2018; Wambura et al., 2018). The simultaneous use of streamflow and RS-ET products can constrain parameter values, and reduce the predictive uncertainty (Herman et al., 2018; Parajuli et al., 2018; Rajib et al., 2018; Wambura et al., 2018). Wambura et al. (2018) demonstrated the usefulness of RS-ET products in reducing the degree of equifinality, which is the tendency for different parameter sets (referred to as PARs hereafter) to produce equally acceptable model outputs (Beven, 2006). A study by Rajib et al. (2018) found substantial improvement in the modeled ET predictions by including vegetation parameters and the utility of RS-ET products in evaluating ET variations across a landscape, indicating a change in the model performance measure, that is the Kling-Gupta Efficiency (KGE) from 0.6 to 0.7. Thus, access to RS-ET products enables the assessment of the model capacity to predict the spatial distribution of hydrologic variables (Becker et al., 2019; Rajib et al., 2018).

Root uptake of water and subsequent transpiration from leaf areas comprise a significant portion of the total ET in vegetated areas. Therefore, its parameterization is crucial for ET simulations. However, previous studies have rarely included vegetation data in the calibration and validation of ET simulations (Herman et al., 2018; Parajuli et al., 2018; Rajib et al., 2018;

Wambura et al., 2018). Ha et al. (2018) applied remotely sensed ET and vegetation data to SWAT modeling, but their study focused only on the usefulness of remotely sensed data for regions without streamflow observations. ET simulations without model calibration against vegetation data can be problematic because SWAT estimates of ET may not accurately reflect the contribution of vegetation. The leaf area index (LAI), referred to as the projected leaf area over a unit of land, is an important vegetation parameter that is closely related to vegetation transpiration (Bian et al., 2019; Gigante et al., 2009). Several studies have emphasized that LAI should be considered for ET predictions because of the strong correlation between ET and LAI (Wang et al., 2010; Yan et al., 2012). The increased availability of remotely sensed LAI (RS-LAI) products provides an opportunity to apply these data to hydrological modeling studies (Andersen et al., 2002; Stisen et al., 2008).

The primary goal of this study was to explore the usefulness of the two remotely sensed datasets, namely RS-ET and RS-LAI, in enhancing watershed model uncertainty for a small watershed (221 km^2) within the coastal plain of the Chesapeake Bay Watershed (CBW). The hydrologic model chosen for this study was SWAT because remotely sensed data have been widely incorporated into this model. To achieve this research goal, this study conducted a lumped parameterization at the watershed level using three constraints: streamflow, RS-ET, and RS-LAI products. The PARs that resulted in acceptable streamflow and ET simulations (referred to as "PARs-1," hereafter) were taken from all PARs explored for calibration. In addition, the PARs with acceptable model performance measures for streamflow, ET, and LAI (referred to as "PARs-2," hereafter) were extracted from all explored PARs. The specific objectives of this study were to: (i) compare the two PARs (i.e., PARs-1 and PARs-2) along with their simulated outputs (e.g., streamflow, ET, and LAI), and explore the role of vegetation constraints (i.e., RS-LAI products)

https://doi.org/10.5194/hess-2022-187
Preprint. Discussion started: 28 June 2022

in improving ET simulations and constraining acceptable PARs; and (ii) test whether those additional constraints (i.e., RS-ET and RS-LAI products) are useful in identifying the PARs that well represent the spatial distribution of ET and LAI.

2. Materials and methods

2.1. Study area

This study was conducted in the Tuckahoe Creek watershed (TCW), upstream of the U.S. Geological Survey (USGS) gauge station #01491500. The watershed is situated as a sub-basin of the Choptank River watershed within the CBW coastal plain (Fig. 1a). The Choptank River watershed has been the focus of intensive research (McCarty et al., 2008) led by the U.S. Department of Agriculture-Natural Resources Conservation Service (USDA-NRCS; Duriancik et al., 2008) and the USDA-Agricultural Research Service (USDA-ARS; Baffaut et al., 2020). The TCW is predominantly covered by croplands (54%), followed by forest (32.8%), pasture (8.4%), urban land (4.2%), and water bodies (0.6%, Fig. 1b). The main crops in the watershed include corn, soybeans, and winter wheat. According to the soil classification system illustrated in the USDA-NRCS, soils are mainly composed of moderately well (Hydrologic Soil Group (HSG) – B, 55.8%) and poorly (HSG – D%, 41.7%) drained soils (Fig. 1c). A detailed description of HSGs is presented in Fig. 1. Based on long-term weather observations from three meteorological stations operated by the National Climate Data Center (NCDC) and the National Oceanic and Atmospheric Administration (NOAA) (Fig. 1a), the annual mean precipitation and daily average temperature for the past 30 years (1985 – 2014) are estimated to be 1166 mm (± 228 mm) and 13 °C (± 1 °C), respectively. The study has a humid subtropical climatic condition affected by the Chesapeake Bay

https://doi.org/10.5194/hess-2022-187
Preprint. Discussion started: 28 June 2022

and the Atlantic Ocean, resulting in fairly uniform precipitation over the course of the year (Fisher et al., 2010). The study site is characterized by flat topography (0 - 32 m above sea level). Irrigation for corn and soybean production during the summer season has seen a substantial increase in this region (Wolman, 2008), which amplifies water loss by ET during the summer season. Water balance cycling in this region is greatly affected by seasonal variations in ET. Thus, an accurate ET simulation for this region is crucial for advancing predictions from hydrological models.

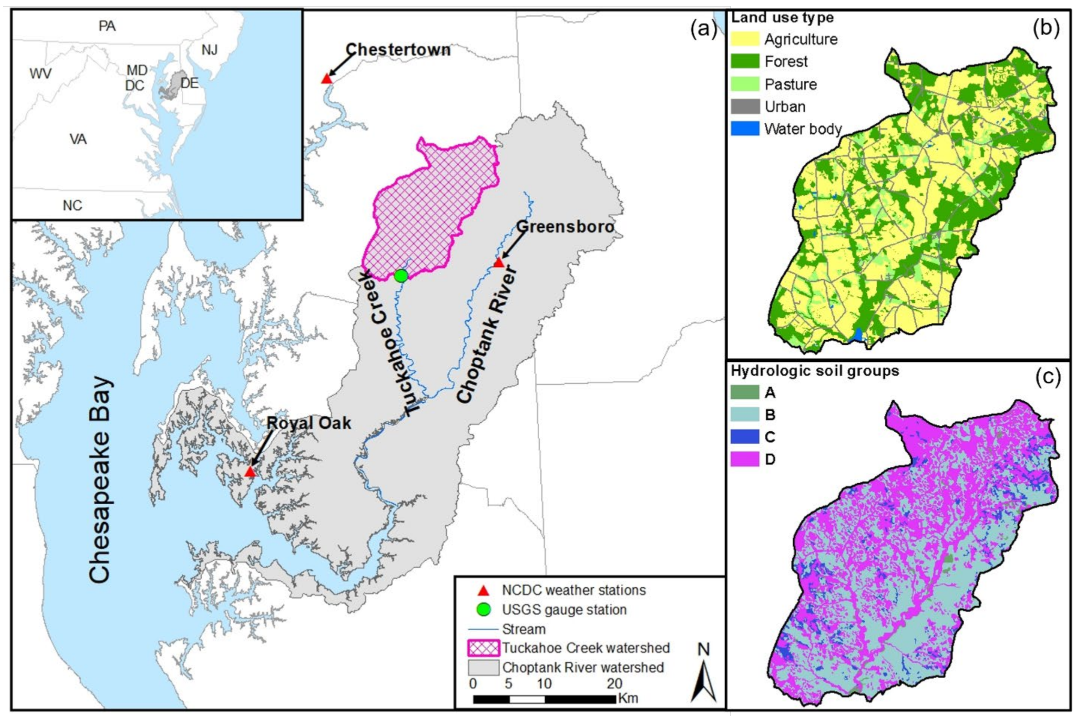

Fig. 1. Characteristics of the study area (Tuckahoe Creek Watershed): (a) location, (b) land use type, and (c) hydrologic soil groups (adapted from Lee et al., 2018a) Note: hydrologic soil groups (HSGs) are characterized as follows: Type A – well-drained soils with 7.6–11.4 mm·h^{-1} water infiltration rate; B – moderately well-drained soils with 3.8–7.6 mm·h^{-1}; C – moderately poorly-drained soils with 1.3–3.8 mm·h^{-1}; and D – poorly-drained soils with 0–1.3 mm·h^{-1} (Neitsch et al., 2011). HSG–A, B, C, and D account for 0.3, 55.8, 2.2, and 41.7% of TCW, respectively.

2.2. Soil and Water Assessment Tool

The SWAT model is a watershed-scale model designed to study the impacts of environmental and anthropogenic changes on hydrological processes within an agricultural watershed (Neitsch et al., 2011). The SWAT includes several components that account for climate, hydrology, nutrients/pesticides, erosion, land cover/plant, management practices, and channel processes (Neitsch et al., 2011). The model partitions a given watershed into sub-watersheds and hydrological response units (HRUs). The HRU is the basic modeling unit and is characterized as a unique combination of land use, soil, and slope within individual sub-watersheds. Hydrologic variables are determined at the individual HRU level, after which outputs are combined at the sub-watershed and watershed levels through channel processes (Neitsch et al., 2011). The cumulative water balance of each HRU is computed using Eq. 1:

$$SW_t = SW_0 + \sum_{i=1}^{t}(R_{day} - Q_{surf} - E_a - W_{seep} - Q_{gw}) \quad (1)$$

Where, SW_t is the final soil water content (mm H_2O), SW_0 is the initial soil water content (mm H_2O), t is the time (days), R_{day} is the amount of precipitation on day i (mm H_2O), Q_{surf} is the amount of surface runoff on day i (mm H_2O), E_a is the amount of ET on day i (mm H_2O), W_{seep} is the amount of percolation and bypass flow at the bottom of the soil profile on day i (mm H_2O), and Q_{gw} is the amount of groundwater flow on day i (mm H_2O). In SWAT, the surface runoff volume is computed using a modified SCS curve number (USDA-SCS, 1972) or the Green and Ampt infiltration method (Green and Ampt, 1911). The former was used in this study.

The SWAT model first calculates potential ET (PET) and then estimates actual ET (AET). Three calculation methods for potential evapotranspiration (PET) are available in the SWAT model (Neitsch et al., 2011): Penman–Monteith (Monteith, 1965), Priestley–Taylor (Priestley and

https://doi.org/10.5194/hess-2022-187
Preprint. Discussion started: 28 June 2022

Taylor, 1972), and Hargreaves (Hargreaves et al., 1985). After computing PET, AET is estimated by considering evaporation on the canopy, soil evaporation, and plant transpiration, which are computed depending on the applied PET method (Neitsch et al., 2011). The actual soil evaporation is determined as a function of soil depth and soil water content. The actual plant transpiration is computed as the reduced optimal plant transpiration due to the limited soil water available for plants.

This study used the Penman–Monteith method, which is expressed in Eq. (2), as follows:

$$\lambda E = \frac{\Delta\cdot(\mathrm{H_{net}} - \mathrm{G}) + \rho_{\mathrm{air}}\cdot \mathrm{c_p}\cdot[\mathrm{e_z^0} - \mathrm{e_z}]/\mathrm{r_a}}{\Delta + \gamma\cdot(1 + \mathrm{r_c}/\mathrm{r_a})} \tag{2}$$

Where, λE is the latent heat of vaporization (MJ kg^{-1}), E the depth rate evaporation (mm d^{-1}), Δ the slope of the saturation vapor pressure-temperature curve (kPa ◦C $^{-1}$), H_{net} the net radiation (MJ m^{-2} d^{-1}), G the ground heat flux density (MJ m^{-2} d^{-1}), ρ_{air} the air density (kg m^{-3}), c_p the specific heat at constant pressure (MJ kg^{-1} ◦C $^{-1}$), e_z^0 the saturation vapor pressure of air at height z (kPa), e_z the water vapor pressure of air at height z (kPa), γ the psychrometric constant (kPa ◦C $^{-1}$), $\mathrm{r_c}$ the plant canopy resistance (s m^{-1}) and $\mathrm{r_a}$ the diffusion resistance of the air layer (aerodynamic resistance) (s m^{-1}).

In SWAT, dynamic LAI estimates are generated as a function of the optimal leaf area development curve. This curve controls LAI growth through accumulated potential heat units. A daily potential heat unit is computed as the difference between the daily average temperature and base temperature. The base temperature is the minimum temperature for vegetation growth, and its default value is set to 0 °C. If the base temperature is greater than the daily average temperature,

https://doi.org/10.5194/hess-2022-187
Preprint. Discussion started: 28 June 2022

the daily heat unit is zero. During the initial growth period, leaf area development is simulated as a function of the optimal leaf area development curve.

$$fr_{LAImx} = \frac{fr_{PHU}}{fr_{PHU} + exp\left(\ell_1 - \ell_2 \cdot fr_{PHU}\right)} \tag{3}$$

Where, fr_{LAImx} is the fraction of the plant's maximum leaf area index corresponding to a given fraction of potential heat units for the plan, fr_{PHU} is the fraction of potential heat units accumulated for the plant on a given day in the growing season, and ℓ_1 and ℓ_2 are the shape coefficients. In the leaf area development curve, once the LAI reaches its (vegetation type-specific) maximum value, the maximum LAI is maintained until leaf senescence begins, after which it was linearly decreased before dormancy (Neitsch et al., 2011).

2.3. Input data and model set-up

The SWAT model requires climate and geospatial data as inputs for simulations (Table 1). Daily precipitation and temperature records from 2008 to 2014 were downloaded from NOAA NCDC monitoring stations (Fig. 1a). Daily solar radiation, relative humidity, and wind speed were prepared using the SWAT model's built-in weather generator (Neitsch et al., 2011) because the three climate data points were not observed by monitoring stations in this region. The nearest station at Greensboro only collected daily precipitation; thus, daily temperature records were obtained from the next closest station at Chestertown from January 2008 to May 2011. As the station at Chestertown collected temperature data only until May 2011, the third nearest station at Royal Oak was chosen to obtain data from June 2011 to December 2014. The calculation of daily solar radiation, relative humidity, and wind speed via weather generator is described in the Text

https://doi.org/10.5194/hess-2022-187
Preprint. Discussion started: 28 June 2022

A2. Digital elevation model (DEM) data was collected by the Maryland Department of Natural Resources (MD-DNR), and the dataset was post-processed by USDA-ARS, Beltsville, in order to use the DEM as input to the SWAT model. Soil map information corresponding to the study area was downloaded from the Soil Survey Geographical Database (SSURGO). A land use map developed by Lee et al. (2016) was used based on the multiple geospatial sources listed in Table 1 (Lee et al., 2016). This map includes eight representative crop rotations (Table 2) with their locations determined by multiyear cropland data layers (CDLs) obtained from the USDA National Agricultural Statistics Service (NASS). Detailed scheduling data are available in Supplementary Material Table S1.

Table 1. List of SWAT model input and calibration data

Data Type	Source	Description	Year
DEM	MD-DNR	LiDAR-based 10-meter resolution	2006
Land Use	USDA-NASS	Cropland Data Layer (CDL)	2008 - 2012
	MRLC	National Land Cover Database (NLCD)	2006
	USDA-FSA-APFO	National Agricultural Imagery Program digital Orthophoto quad imagery	1998
	US Census Bureau	TIGER road map	2010
Soils	USDA-NRCS	Soil Survey Geographical Database (SSURGO)	2012
Climate	NCDC	Daily precipitation and temperature	2008 – 2014
Streamflow	USGS	Monthly streamflow	2008 – 2014
RS-ET	Sun et al. (2017)	Daily ET	2010 – 2014
RS-LAI	NASA USDA-ARS	Daily LAI	2010 – 2014

MRLC: Multi-Resolution Land Characteristics Consortium, USDA-FSA-APFO: USDA-Farm Service Agency-Aerial Photography Field Office, and TIGER: Topologically Integrated Geographic Encoding and Referencing. Detailed values (average, minimum and maximum) of precipitation, temperature, streamflow, RS-ET and –LAI are available in the Table A1.

https://doi.org/10.5194/hess-2022-187
Preprint. Discussion started: 28 June 2022

Table 2. Eight representative cropland rotations used in the SWAT simulations.

Type	2008	2009	2010	2011	2012	2013	2014	Proportion
1	WW/Soyb	Corn	WW/Soyb	Corn	WW/Soyb	Corn	WW/Soyb	14.5
2	Corn	WW/Soyb	Corn	WW/Soyb	Corn	WW/Soyb	Corn	21.9
3	WW/Soyb	Corn	Soyb	Corn	WW/Soyb	Corn	Soyb	7.7
4	Soyb	Corn	Soyb	Corn	Soyb	Corn	Soyb	11.3
5	Corn	Soyb	Corn	Soyb	Corn	Soyb	Corn	9.8
6	Corn	Corn	Corn	Corn	Corn	Corn	Corn	17.1
7	Corn	Soyb	Soyb	Corn	Soyb	Soyb	Corn	10.2
8	Soyb	Corn	Soyb	Soyb	Corn	Soyb	Soyb	7.5
Corn	59	58	49	61	56	51	59	56
Soyb	41	42	51	39	44	49	41	44

WW/Soyb and Soyb indicate double-crop winter wheat, soybeans, and soybeans, respectively. The last column indicates the relative area (%) of each crop rotation applied to the croplands. The bottom two rows indicate the relative areas (%) of the corn and soybean fields resulting from different concurrent rotations.

Daily streamflow records from 2010 to 2014 were obtained from USGS gauging station #01491500, located at the outlet of the TCW (Fig. 1a). Daily RS-ET products were generated from the regional Atmosphere-Land Exchange Inverse (ALEXI) model (Anderson et al., 1997, 2007) and the associated flux spatial-temporal disaggregation scheme (DisALEXI) (Anderson et al., 2004). This multiscale modeling system is based on the two-source energy balance model (Norman et al., 1995), which uses remotely sensed land surface temperature (LST) observations to partition the available energy between latent and sensible heat fluxes from the soil and canopy components of a scene. A data fusion algorithm can be used to fuse 30 m resolution/bi-weekly ET retrievals from Landsat LST observations with 500 m/daily data from MODIS, which results in fused datasets with both high spatial and temporal resolutions (Anderson et al., 2018; Cammalleri et al., 2013, 2014). Over the study area, 30 m daily RS-ET products from ALEXI/DisALEXI were validated against in-situ eddy covariance flux tower measurements with an average relative error of 10% (Sun et al., 2017). The RS-ET products used in this study covered the period from January 2010 to December 2014.

https://doi.org/10.5194/hess-2022-187
Preprint. Discussion started: 28 June 2022

The daily LAI with 500 m spatial resolution was generated from the MODIS Version 6 LAI/FPAR products (MCD15A3H). MCD15A3H is a combined LAI product from two satellites (Terra and Aqua) at a 4-day temporal frequency. For this study, MODIS LAI data products were downloaded from the National Aeronautics and Space Administration (NASA) and reprocessed to the daily LAI in the USDA-ARS, Beltsville. The daily LAI values were obtained in two steps. First, MODIS LAI quality control (QC) layers (FparLai_QC and FparExtra_QC) were used to exclude LAI retrievals from partial clouds, cloud shadows, and dead detectors. Furthermore, LAI retrievals from the physical radiative-transfer model (main algorithm) and empirical model (backup algorithm) (Myneni et al., 2002) were separated. Second, the 4-day MODIS LAI data from the first step were smoothed and interpolated to daily LAI values using the Savitzky–Golay (SG) filter approach (Savitzky and Golay, 1964) with a flexible fitting strategy (Gao et al., 2020). Daily LAI values at a 500 m spatial resolution from 2010 to 2014 were generated for this study. RS-ET and RS-LAI samples are shown in Fig. S1 of the Supplementary Material.

The study watershed was divided into 19 sub-watersheds that ranged between 0.09 and 32 km^2. In the HRU generation process, the threshold area values of land use, soil, and slope were set to >10%, >15%, and >15%, respectively. There were 542 HRUs (312 cropland HRUs and 39 forest HRUs) in TCW. The size of the HRUs ranged from 10^{-6} to 7.21 km^2, with an average size of 0.41 km^2.

2.4. Model calibration/validation and spatial evaluation

Model simulations were performed at a daily time step from 2008 to 2014, given the availability of RS-ET (2010–2014). The SWAT model was calibrated against three datasets: observed streamflow, watershed-level RS-ET, and RS-LAI. The first two years (2008–2009) were

https://doi.org/10.5194/hess-2022-187
Preprint. Discussion started: 28 June 2022

used as the spin-up periods. Three years (2010–2012) were set aside for the model calibration. Model validation was performed for the remaining two years (2013–2014). At the watershed level, model calibration was performed using streamflow, watershed-level RS–ET and RS–LAI, after which PARs-1 (acceptable for streamflow and RS-ET) and PARs-2 (acceptable for streamflow, RS-ET, and RS-LAI) were determined (Section 2.4.1). Then, a spatial evaluation was conducted at the sub-watershed (section 2.4.2) using simulations from PARs-2.

2.4.1. Watershed-level calibration

Numerous studies have applied the SWAT in this study area (Lee et al., 2019; Sharifi et al., 2016; Shirmohammadi et al., 2006; Yeo et al., 2019). These studies showed sensitive parameters with ranges and optimal values satisfying acceptable performance measures, as summarized by Moriasi et al., 2007). Based on previous studies, we selected 13 hydrologic parameters that were shown to be sensitive in this region. In addition to the hydrologic parameters, seven vegetation parameters were selected to calibrate the LAI values of corn, soybean, and forest; these vegetation parameters were derived from previous studies that calibrated crops and forests (Yang and Zhang, 2016; Yeo et al., 2014). The tree vegetation types were considered in calibration because they accounted for more than 90% of the watershed. In addition, corn and soybean parameters were adjusted because the distribution and rotation of the two crops were well captured by the land use map used in this study. The detailed practice schedules (e.g., the application timing and amount of fertilizer, planting, and harvesting timings) of the two crops were developed by local experts (Lee et al., 2016). Thus, the growth dynamics of corn and soybean were depicted in our simulations. The double crop soybean was not calibrated as all the information described above was made for summer crops. Table 3 lists the calibrated parameters and allowable ranges.

https://doi.org/10.5194/hess-2022-187
Preprint. Discussion started: 28 June 2022

Table 3. Description and ranges of calibrated parameters

Parameter	Description (units)	Range
CN$^{!}$	SCS runoff curve number	-20 – 20%
GW_DELAY$^{!}$	Groundwater delay (days)	0 – 500
ALPHA_BF$^{!}$	Baseflow alpha factor (days^{-1})	0 – 1
GWQMN$^{!}$	Threshold depth of water in the shallow aquifer required for return flow to occur (mm H_2O)	0 – 5000
GW_REVAP$^{!}$	Groundwater "revap" coefficient	0.02 – 0.2
REVAPMN$^{!}$	Threshold depth of water in the shallow aquifer for "revap" to occur (mm H_2O)	0 – 1000
SOL_AWC$^{!}$	Available water capacity of the soil layer (mm H_2O ·mm soil^{-1})	-50 – 50%
CH_K2*	Effective hydraulic conductivity in the main channel alluvium	0 – 500
CH_N2*	Manning's "n" value for the tributary channels	0.01 – 0.3
SURLAG$^{\$}$	Surface runoff lag coefficient	0.5 – 24
ESCO$^{!}$	Soil evaporation compensation factor	0 – 1
EPCO$^{!}$	Plant uptake compensation factor	0 – 1
CANMX$^{!}$	Maximum canopy storage (mm H_2O)	0 – 100
BIO_E$^{!}$ (corn, soybean, forest)	Radiation use efficiency in ambient CO_2 ((kg/ha)/(MJ/m^2))	10 – 90
BLAI$^{!}$ (corn, soybean, forest)	Maximum potential leaf area index (m^{2}m^{-2})	0.5 – 10
FRGRW1$^{!}$ (corn, soybean, forest)	Fraction of the plant growing season of total potential heat units corresponding to the first point on the leaf area development curve	0 – 0.5
FRGRW2$^{!}$ (corn, soybean, forest)	Fraction of the plant growing season of total potential heat units corresponding to the second point on the leaf area development curve	0.5 – 1
LAIMX1$^{!}$ (corn, soybean, forest)	Fraction of the maximum leaf area index corresponding to the first point on the leaf area development curve	0 – 0.5
LAIMX2$^{!}$ (corn, soybean, forest)	Fraction of the maximum leaf area index corresponding to the second point	0.5 – 1
DLAI$^{!}$ (corn, soybean, forest)	Leaf to biomass fraction	0.15 – 1.00

Note: !, *, and $ indicate the parameters whose values differ by the hru, sub-watershed, and watershed levels.

For model calibration, 20,000 PARs were prepared using Latin hypercube sampling (LHS). The LHS method divides the sampling space of individual parameters into multiple non-overlapping subspaces with equal probabilities (McKay et al., 2000). Then, the LHS generates one PAR by randomly selecting individual parameter values within each subspace, while forcing each subspace to have only one value for each PAR (McKay et al., 2000). LHS is known to effectively converge to the optimal PAR relative to random sampling (Wambura et al., 2018).

After each simulation, three daily model outputs (streamflow, ET, and LAI) were simultaneously compared with the corresponding observations. For this study, we selected KGE as the model performance measure, as it was widely adopted in SWAT modeling studies that applied RS-ET and RS-LAI. Furthermore,

$$KGE = 1 - \sqrt{(r-1)^2 - (\sigma_s/\sigma_o - 1)^2 - (\mu_s/\mu_o - 1)^2} \quad (4)$$

Where, r indicates the Pearson product-moment correlation coefficient, σ_s/σ_o and μ_s/μ_o indicate the variability ratio and bias between simulations and observations, respectively, σ and μ are the standard deviation and mean of the variables, respectively. The subscripts s and o indicate simulations and observations, respectively. The KGE values range from $-\infty$ to 1, with values closer to 1 indicating stronger model performance.

KGE was calculated using the "hydroeval" package of the Python 3.8.12 program (Hallouin, 2020). This study defined acceptable daily model performance measures as follows: streamflow (KGE > 0.55, NSE >), ET, and LAI (KGE > 0.5). Using previous studies (Becker et al., 2019; Poméon et al., 2018), relaxed criteria were set for ET and LAI relative to the streamflow.

2.4.2. Spatial evaluation at sub-watershed level

The simulated ET and LAI were compared with RS-ET and RS-LAI products at the sub-watershed level. The RS-ET and RS-LAI products were discretized by the sub-watershed boundary generated from the ArcSWAT interface using the input DEM (Winchell et al., 2007). The TCW included 19 sub-watersheds. Except for one sub-watershed that was smaller than the LAI pixel size (0.25 km^2), 18 sub-watersheds were used for the sub-watershed-level spatial evaluation. This evaluation was conducted using PARs-1 and PARs-2 simulations. Furthermore, the KGE values were computed for ET and LAI for individual sub-watersheds and the median KGE values. The PARs with median KGE values greater than 0.5 for both ET and LAI were considered to represent

https://doi.org/10.5194/hess-2022-187
Preprint. Discussion started: 28 June 2022

acceptable performance measures for the spatial distribution of ET and LAI at the sub-watershed level. PARs that did not meet these criteria were viewed as unable to capture the spatial distribution of ET and LAI at the sub-watershed level, although they showed acceptable performance at the watershed level. The evaluation results were used to further assess the degree of equifinality.

3. Results and discussions

3.1. Impacts of vegetation data on ET predictions and predictive uncertainty at the watershed level

The watershed-level calibration results show that there were 14 PARs-1 and 6 PARs-2 (Table 4). The ranges of KGE values for PARs-1 were 0.59–0.77 (0.56–0.62) for streamflow and 0.50–0.60 (0.56–0.61) for RS-ET during calibration (and validation) periods (Table 4). The six PARs (PARs-2) were observed to simultaneously satisfy the model performance thresholds for streamflow, RS-ET, and RS-LAI (Table 4). The model performance measures for PARs-2 were 0.59–0.73 (0.56–0.59) for streamflow, 0.51–0.56 (0.57–0.58) for RS-ET, and 0.51–0.62 (0.57–0.77) for RS-LAI during calibration (and validation) periods.

The degree of equifinality was reduced from 14 to 6 with the inclusion of the RS-LAI. Although RS-LAI was incorporated, a 50% reduction in equifinality was observed because both the ET calculation and RS-ET considered the LAI. The ET calculation method in this study (Penman-Monteith) used canopy resistance as a key variable, which was calculated from the LAI in SWAT (Neitsch et al., 2011). RS-LAI data were used as inputs for RS-ET retrievals (Sun et al., 2017). Therefore, calibrated parameter sets that matched RS-ET could also perform well with respect to LAI estimation. A previous study by Chen et al. (2017) also reported a high correlation between ET and LAI from the SWAT results.

Table 4. Performance measures (KGE value) for daily streamflow, RS-ET, and RS-LAI

	Streamflow		RS-ET		RS-LAI	
	Calibration	Validation	Calibration	Validation	Calibration	Validation
1	0.71	0.60	0.53	0.57	0.45	0.55
2	0.73	0.56	0.51	0.58	0.10	0.11
3	0.73	0.56	0.54	0.58	0.55	0.69
4	0.66	0.57	0.56	0.57	0.58	0.67
5	0.77	0.60	0.52	0.59	0.50	0.57
6	0.66	0.62	0.55	0.56	0.41	0.43
7	0.63	0.57	0.52	0.57	0.27	0.29
8	0.68	0.59	0.50	0.56	0.48	0.55
9	0.59	0.59	0.53	0.58	0.51	0.57
10	0.60	0.58	0.60	0.61	0.22	0.34
11	0.72	0.59	0.56	0.57	0.48	0.57
12	0.60	0.58	0.53	0.58	0.57	0.70
13	0.68	0.56	0.51	0.57	0.62	0.77
14	0.63	0.58	0.52	0.58	0.56	0.69

Note: The six rows (#3, 4, 9, 12, 13, and 14) are PARs-2.

The observed streamflow, RS-ET, and RS-LAI were plotted against the simulation results from PARs-2 (Fig. 2). The simulated streamflow did not capture the observed peak flows during the simulation period. This may be because the precipitation data collected at the weather stations did not fully represent the spatial variations in meteorological conditions across the entire study site. Localized variations in precipitation have frequently been observed in this study area, which may have further contributed to the underestimation of the peak streamflow (Lee et al., 2016; Yeo et al., 2014). Spatially continuous climatic data, including the North American Land Data Assimilation System (NLDAS) and the Next-Generation Radar (NEXRAD), have been shown to

https://doi.org/10.5194/hess-2022-187
Preprint. Discussion started: 28 June 2022

reduce prediction uncertainty from climatic data taken from stations (Qi et al., 2019; Sexton et al., 2010). The use of these data may better mimic the peak streamflow. The ET and LAI results showed strong seasonal trends with high values during the summer season (May to October) and low values during the winter season (November to April). This was in agreement with an earlier study by Fisher et al. (2010) and local tower measurements (Sun et al., 2017). Warm temperatures and plant growth led to peak ET and LAI values during the summer period.

https://doi.org/10.5194/hess-2022-187
Preprint. Discussion started: 28 June 2022

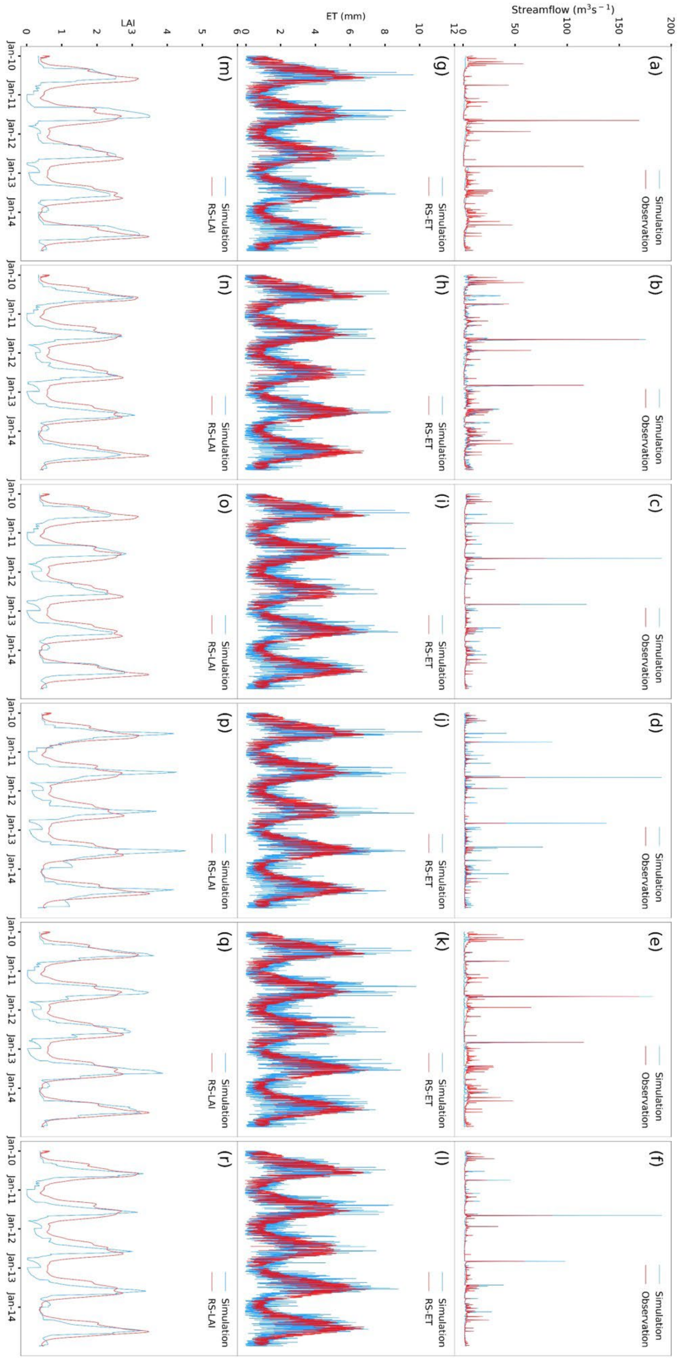

Fig. 2. Comparison of daily simulations with observed streamflow, watershed-level RS-ET, and RS-LAI during the simulation period from 2010 to 2014: PAR #3 (a, g, and m), #4 (b, h, and n), #9 (c, i, and o), #12 (d, j, and p) #13 (e, k, and q) #14 (f, l, and r). The unit of LAI is $m^2 \cdot m^{-2}$.

https://doi.org/10.5194/hess-2022-187
Preprint. Discussion started: 28 June 2022

Hydrology and Earth System Sciences
Discussions

As compared to streamflow and RS-LAI, low KGE values were observed in the ET simulations (Fig. 2). Low accuracy of ET in this study was likely attributable to the exclusion of irrigation practices in our simulations because of inadequate associated information, whereas the thermal ET remote sensing approach directly captured the impact of irrigation on ET (Hain et al., 2015). A previous study found that improved ET simulation resulted from the inclusion of irrigation practices in the simulations (Chen et al., 2017). Depressional wetlands, which are abundant in forested areas of this region, are likely to lose water via ET at rates higher than those captured by the SWAT model. Therefore, the ET module in the forested settings could have been an additional factor that led to low KGE values of ET (Fig. 2). Simulated LAI values were mostly lower than observations during the winter season (Fig. 2). Winter cover crops are widely implemented in this region to reduce nutrient loads. These crops have been shown to increase the winter vegetation index (Hively et al., 2020). The omission of winter cover crops from the simulation used in this study resulted in a low simulated LAI during the summer season.

3.2. Comparing model results with RS-ET and RS-LAI at the sub-watershed level

Sub-watershed-level KGE values were calculated for daily ET and LAI, as shown in Fig. 3. The median KGE values for ET ranged from 0.51 to 0.55 and from 0.57 to 0.58 during the calibration and validation periods, respectively. Lower KGE values were observed for LAI predictions (0.46–0.57 for the calibration period and 0.54–0.57 for the validation period) relative to ET predictions. All PARs-2 showed acceptable performance measures for the sub-watershed-level ET criteria, but only three PARs-2 (#4, #13, and #14) exceeded the sub-watershed-level LAI criteria (KGE > 0.5).

https://doi.org/10.5194/hess-2022-187
Preprint. Discussion started: 28 June 2022

The PAR#12 case was associated with high KGE values for LAI (0.57 and 0.70 for the calibration and validation periods, respectively) at the watershed level, but its KGE values at the sub-watershed level were 0.46 and 0.54 for the the calibration and validation periods, respectively (Figs. 2 and 3). Similar to the PAR#12 case, the PAR#3 and #9 cases exhibited acceptable KGE values at the watershed level and narrowly failed to meet the sub-watershed-level criteria for LAI. With respect to the sub-watershed results, the number of acceptable PARs decreased from six (PARs-2) to three, which suggested that the sub-watershed-level assessment helped identify the PARs that satisfactorily characterized internal processes at a finer spatial level. This finding supports the conclusion that spatial assessment using remotely sensed data can further narrow the acceptable PARs, thus reducing predictive uncertainty (e.g., equifinality).

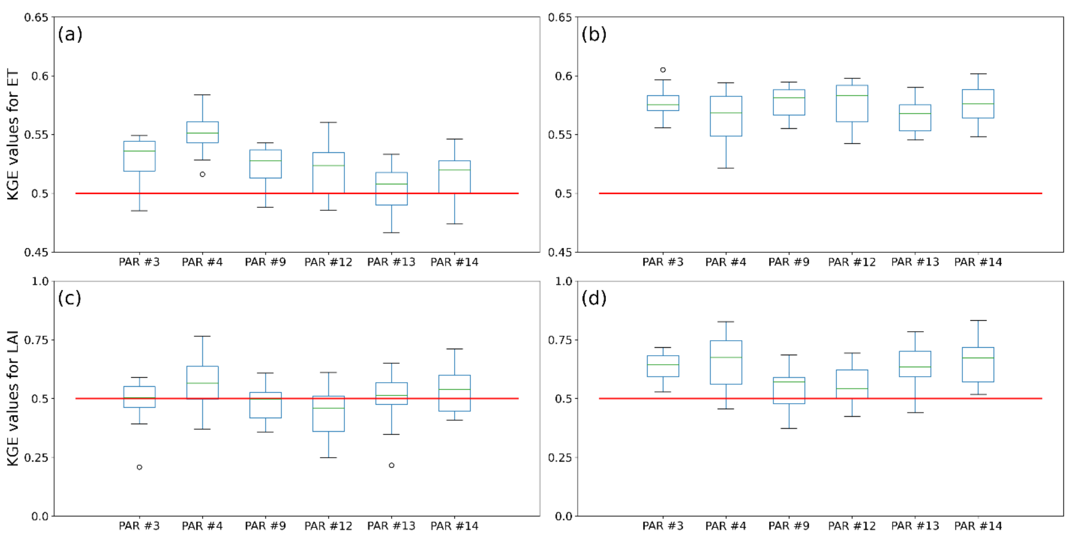

Fig. 3. Median KGE values of sub-watersheds: (a) ET for calibration periods, (b) ET for validation periods, (c) LAI for calibration periods, (a) LAI for validation periods. The horizontal red line indicates a KGE threshold value of 0.5. KGE values of ET and LAI for individual sub-watersheds are available in the supplementary material Tables S2 and S3, respectively.

https://doi.org/10.5194/hess-2022-187
Preprint. Discussion started: 28 June 2022

Hydrology and Earth System Sciences
Discussions
Open Access

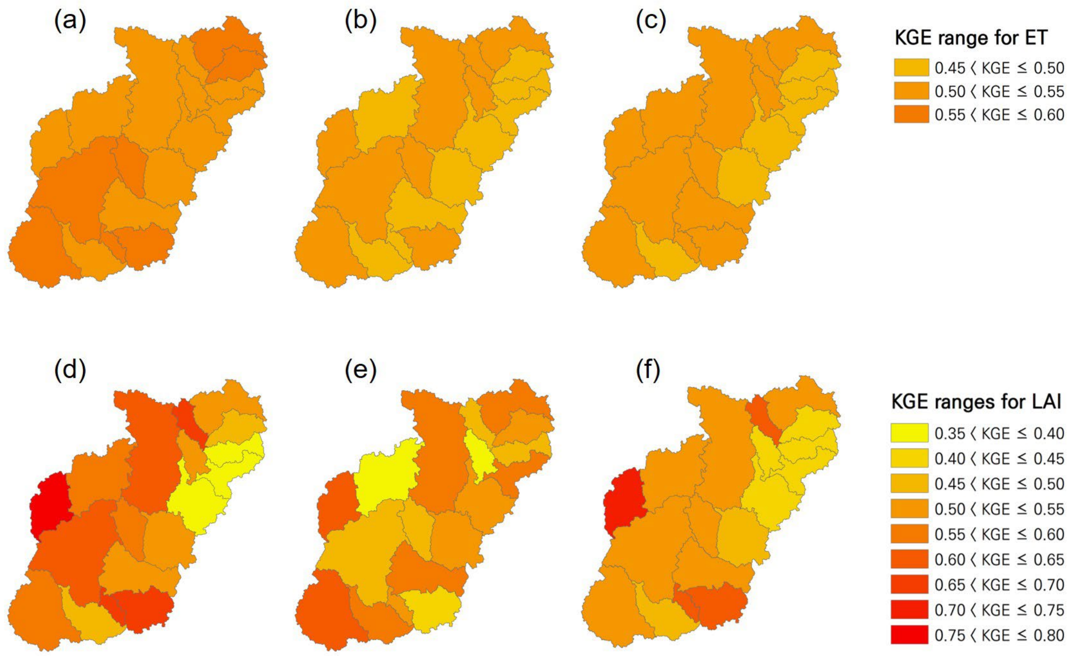

Fig. 4. Spatial distribution of KGE values for the PAR#4, PAR#13, and PAR#14 cases at the sub-watershed level for ET (a, b, and c) and LAI (d, e, and f).

At the sub-watershed level, half of the PARs-2 were acceptable for LAI, whereas all PARs-2 met the sub-watershed-level ET criterion. This was likely due to the spatial resolution of the RS-ET and RS-LAI. RS-ET with a 30 m resolution might better represent the sub-watershed-level ET, but RS-LAI with a 500 m resolution might not discern the sub-watershed-level LAI from the watershed-level value.

Although spatialized parameterization requires large computational resources and long simulation times, it is useful for characterizing large watersheds (Becker et al., 2019; Rajib et al., 2018). However, relative to the spatial extent of those studies (> 1670 km^2), the spatial extent of our study site (220 km^2) was small. Moreover, this study focused on the use of multiple remotely

https://doi.org/10.5194/hess-2022-187
Preprint. Discussion started: 28 June 2022

sensed datasets to reduce predictive uncertainty. Therefore, the lumped parameterization used in this study was sufficient to assess the prediction accuracy of the spatial distributions of ET and LAI.

4. Limitations and implications

This study aimed to improve model predictions by accommodating remotely sensed ET and LAI in an effort to contribute to watershed modeling. However, this study had several limitations to be conisdered for future studies. Remotely sensed data inevitably include uncertainties that are greater than those in observations collected at the watershed outlet (Vervoort et al., 2014) but they also enable hydrological models to be evaluated at a finer spatial level than watersheds (Rajib et al., 2018). Thus, the uncertainty embedded in remotely sensed data must be carefully considered when incorporating remotely sensed data into watershed modeling. Furthermore, simulated ET and LAI are highly influenced by the climatic data. In this study, three sets of climatic input data (i.e., humidity, solar radiation, and wind speed) were prepared using SWAT's built-in weather generator. This has also been practiced in previous studies (Wu and Xu, 2006; Yeo et al., 2014; Zhao et al., 2020). Grid-format continuous climate data are increasingly available and have been adopted in watershed modeling (Basso et al., 2020; Dosdogru et al., 2020). Application of continuous climatic data to half of the generated data can improve the model predictions of ET and LAI. Furthermore, poor simulations (e.g., peak flows) resulting from localized precipitation events can be addressed by incorporating these climatic datasets.

Model performance measures for water quantity and quality variables have been well demonstrated (Moriasi et al., 2007). The measures for ET and LAI varied by temporal scales. Daily

https://doi.org/10.5194/hess-2022-187
Preprint. Discussion started: 28 June 2022

Hydrology and Earth System Sciences
Discussions

simulations of ET and LAI were frequently assessed using only one measure (e.g., KGE) (Rajib et al., 2018, 2020). In case of monthly simultions, multiple measures including Nash-Sutcliffe efficiency [NSE], Percent bias [PBIAS], root mean squared error (RMSE)-observations standard deviation ratio [RSR], KGE, etc, were used (Ding and Zhu, 2022; Haas et al., 2022; Herman et al., 2018; Lee et al., 2022; Parajuli et al., 2018). Depending on the temporal scales of the simulated results, less strict measures were recommended for the streamflow predictions (Arnold et al., 2012). However, the selection of performance measures for ET and LAI has not been well explored. The use of remotely sensed products in watershed modeling is incresing. Therefore, the guideline of the performance measures for variables calibrated against remotely sensed products would be needed.

5. Summary and Conclusion

Hydrological models tackle uncertainty issues caused by incomplete model structures and poor observational data. To address this issue, remotely sensed products have been employed as additional constraints to enhance the prediction accuracy of hydrological models. For example, the use of RS-ET retrievals as additional constraints has led to a substantial reduction in predictive uncertainty and achievement of spatial evaluation. However, vegetation parameters that affect ET dynamics are often adjusted only against RS-ET. This calibration practice may inaccurately represent the impact of vegetation on ET. This study employed RS-LAI as an additional constraint to control vegetation parameters, and explored whether the addition of RS-LAI was beneficial in reducing parameter uncertainty. The SWAT model was calibrated against the observed streamflow and RS-ET, and the calibrated model was further constrained by RS-LAI to determine the number

https://doi.org/10.5194/hess-2022-187
Preprint. Discussion started: 28 June 2022

Hydrology and Earth System Sciences
Discussions

of acceptable parameter sets depending on the presence or absence of RS-LAI as a constraint. Depiction of the spatial distribution of ET and LAI at the sub-watershed level by parameter sets (acceptable for streamflow, ET, and LAI at the watershed level) was further tested. This finer-level evaluation was effective in constraining acceptable parameter sets.

Our results showed that the number of acceptable parameter sets was reduced from 14 to 6 with the inclusion of the RS-LAI. Therefore, the calibrated model against RS-ET and RS-LAI was useful in reducing the degree of equifinality, as compared with the model calibrated against only RS-ET. Among the six parameter sets, only three represented the spatial distribution of ET and LAI at the sub-watershed level with acceptable model performance. This indicates that the equifinality of the hydrological model is further constrained by the spatial evaluation performed in this study. Moreover, RS-LAI was the key constraint at the sub-watershed level, whereas RS-ET rarely limited the parameter sets. This is likely because RS-LAI retrievals are obtained with a low spatial resolution (e.g., 500 m), including high uncertainty in capturing spatialized characteristics relative to RS-ET (e.g., 30 m). Therefore, an inaccurate spatial distribution of LAI might be less efficient in constraining acceptable parameter sets. This suggests that the spatial resolution of the remotely sensed data should be carefully selected based on the spatial extent of the study site.

Overall, this study showed that the predictive uncertainty was affected by the inclusion of RS-LAI at the watershed level. Remotely sensed products enabled hydrologic modelers to conduct spatial evaluations at finer spatial scales, which led to a reduction in the predictive uncertainty and improved representations of intra-watershed processes. These findings emphasized the importance of incorporating remotely sensed data as additional constraints to address the uncertainty in watershed models, thereby extending the usefulness of these models.

https://doi.org/10.5194/hess-2022-187
Preprint. Discussion started: 28 June 2022

Hydrology and Earth System Sciences
Discussions

Appendix A

Table A1. Observed daily minimum and maximum values of precipitation, temperature, streamflow, remotely sensed evapotranspiration (RS-ET) and leaf area index (RS-LAI) products for calibration/validation periods

	Calibration (2010 – 2012)	Validation (2013 – 2014)
Precipitation (mm)	0 – 238 (10)	0 – 125 (10)
Temperature (℃)	-18 – 33 (12)	-9 – 31 (14)
Streamflow (m^3/s)	0.14 – 169 (3.42)	0.70 – 47 (3.69)
RS-ET (mm)	0.03 – 6.84 (2.59)	0.35 – 6.86 (2.76)
RS-LAI (m^3/m^3)	0.38 – 3.18 (1.39)	0.38 – 3.18 (1.39)

Note: A number indicates the minimum (left) and maximum (right) values. The value in the parenthesis is the daily average. The precipitation average only considers values during rainy days (375 and 276 days for calibration and validation periods, respectively).

Text A2. The calculation of solar radiation, relative humidity, by a weather generator

SWAT's built-in weather generator computes solar and relative humidity by a function of precipitation and temperature. Solar radiation and relative humidity are determined based on the number of dry or wet days per given month. Solar radiation is assumed to be lower on wet day (R_w) and that the wet day solar radiation is the half of the dry day solar radiation (R_D).

$$R_w = 0.5 \cdot R_D \quad (1)$$

$$R_D = \frac{R_M \cdot days_T}{5 \cdot days_w + days_D} \quad (2)$$

Where, R_w is the average daily solar radiation for the month, $days_T$ is the total number of days in the month, $days_W$ and $days_D$ are the total number of wet and dry days in the month, respectively.

To incorporate the effect of clear and overcast weather on generated values of relative humidity, monthly average relative humidity values can be adjusted for wet or dry conditions. The wet day average relative humidity is assumed to be greater than the dry day relative humidity by some fraction as Eq. (3). The dry day relative humidity is computed as shown in Eq. (4).

https://doi.org/10.5194/hess-2022-187
Preprint. Discussion started: 28 June 2022

$$R_{hWmon} = R_{hDmon} + b_H \cdot (1 - R_{hDmon}) \tag{3}$$

$$R_{hDmon} = \left(R_{hmon} - b_H \cdot \frac{days_{wet}}{days_{tot}}\right) \cdot \left(1.0 - b_H \cdot \frac{days_{wet}}{days_{tot}}\right)^{-1} \tag{4}$$

Where, R_{hWmon} is the average relative humidity of the month on wet days, R_{hDmon} is the average relative humidity of the month on dry days, b_H is a scaling factor that controls the degree of deviation in relative humidity caused by the presence or absence of precipitation, R_{hmon} is the average relative humidity for the month, $days_{wet}$ and $days_{tot}$ are the number of wet days in the month and the total number of days in the month, respectively.

Wind speed is generated for the potential evapotranspiration by the Penman-Monteith equation. Mean daily wind speed is generated using the equation below.

$$W = \mu wnd_{mon} \cdot (-\ln(rnd_1))^{0.3} \tag{5}$$

Where, W is the mean wind speed for the day ($m \cdot s^{-1}$), μwnd_{mon} is the average wind speed for the month ($m \cdot s^{-1}$), and rnd_1 is a random number between 0.0 and 1.0.

Acknowledgments

This work was supported by the Basic Study and Interdisciplinary R&D Foundation Fund of the University of Seoul (2021) for Sangchul Lee. This research was also supported by the National Research Foundation of Korea (NRF) grant funded by the Korean government (MIST) (No. 2021R1C1C1006030) for Dongho Kim, and the United States Department of Agriculture (USDA) Natural Resources Conservation Service, in association with the Wetland Component of the National Conservation Effects Assessment Project. This research was a contribution from the Long-Term Agroecosystem Research (LTAR) network. LTAR is supported by the USDA.

Disclaimer

The U.S. Department of Agriculture is an equal opportunity provider and employer. Any use of trade, firm, or product names is for descriptive purposes only and does not imply endorsement by the U.S. Government.

https://doi.org/10.5194/hess-2022-187
Preprint. Discussion started: 28 June 2022

References

Andersen, J., Dybkjaer, G., Jensen, K. H., Refsgaard, J. C. and Rasmussen, K.: Use of remotely sensed precipitation and leaf area index in a distributed hydrological model, J. Hydrol., 264(1–4), 34–50, doi:10.1016/S0022-1694(02)00046-X, 2002.

Anderson, M., Gao, F., Knipper, K., Hain, C., Dulaney, W., Baldocchi, D., Eichelmann, E., Hemes, K., Yang, Y., Medellin-Azuara, J. and Kustas, W.: Field-scale assessment of land and water use change over the California delta using remote sensing, Remote Sens., 10(6), 889, doi:10.3390/rs10060889, 2018.

Anderson, M. C., Norman, J. M., Diak, G. R., Kustas, W. P. and Mecikalski, J. R.: A two-source time-integrated model for estimating surface fluxes using thermal infrared remote sensing, Remote Sens. Environ., 60(2), 195–216, doi:10.1016/S0034-4257(96)00215-5, 1997.

Anderson, M. C., Norman, J. M., Mecikalski, J. R., Torn, R. D., Kustas, W. P. and Basara, J. B.: A multiscale remote sensing model for disaggregating regional fluxes to micrometeorological scales, J. Hydrometeorol., 5(2), 343–363, doi:10.1175/1525-7541(2004)005<0343:AMRSMF>2.0.CO;2, 2004.

Anderson, M. C., Norman, J. M., Mecikalski, J. R., Otkin, J. A. and Kustas, W. P.: A climatological study of evapotranspiration and moisture stress across the continental United States based on thermal remote sensing: 1. Model formulation, J. Geophys. Res. Atmos., 112, D10117, doi:10.1029/2006JD007506, 2007.

Arnold, J. G., Moriasi, D. N., Gassman, P. W., Abbaspour, K. C., White, M. J., Srinivasan, R., Santhi, C., Harmel, R. D., Van Griensven, A., Van Liew, M. W., Kannan, N. and Jha, M. K.: SWAT: Model use, calibration, and validation, Trans. ASABE, 55(4), 1491–1508, 2012.

Arnold, J. G., Youssef, M. A., Yen, H., White, M. J., Sheshukov, A. Y., Sadeghi, A. M., Moriasi, D. N., Steiner, J. L., Amatya, D. M., Skaggs, R. W., Haney, E. B., Jeong, J., Arabi, M. and Gowda, P. H.: Hydrological processes and model representation: Impact of soft data on calibration, Trans. ASABE, 58(6), 1637–1660, doi:10.13031/trans.58.10726, 2015.

Baffaut, C., Baker, J. M., Biederman, J. A., Bosch, D. D., Brooks, E. S., Buda, A. R., Demaria, E. M., Elias, E. H., Flerchinger, G. N., Goodrich, D. C., Hamilton, S. K., Hardegree, S. P., Harmel, R. D., Hoover, D. L., King, K. W., Kleinman, P. J., Liebig, M. A., McCarty, G. W., Moglen, G. E., Moorman, T. B., Moriasi, D. N., Okalebo, J., Pierson, F. B., Russell, E. S., Saliendra, N. Z., Saha, A. K., Smith, D. R. and Yasarer, L. M. W.: Comparative analysis of water budgets across the U.S. long-term agroecosystem research network, J. Hydrol., 588, 125021, doi:10.1016/j.jhydrol.2020.125021, 2020.

Basso, M., Vieira, D. C. S., Ramos, T. B. and Mateus, M.: Assessing the adequacy of SWAT model to simulate postfire effects on the watershed hydrological regime and water quality, L. Degrad. Dev., 31(5), 619–631, doi:10.1002/ldr.3476, 2020.

Becker, R., Koppa, A., Schulz, S., Usman, M., aus der Beek, T. and Schüth, C.: Spatially distributed model calibration of a highly managed hydrological system using remote sensing-derived ET data, J. Hydrol., 577, 123944, doi:10.1016/j.jhydrol.2019.123944, 2019.

Beven, K.: A manifesto for the equifinality thesis, in Journal of Hydrology, pp. 18–36., 2006.

Bian, Z., Gu, Y., Zhao, J., Pan, Y., Li, Y., Zeng, C. and Wang, L.: Simulation of evapotranspiration based on leaf area index, precipitation and pan evaporation: A case study of Poyang Lake watershed, China, Ecohydrol. Hydrobiol., 19(1), 83–92, doi:10.1016/j.ecohyd.2018.03.005, 2019.

https://doi.org/10.5194/hess-2022-187
Preprint. Discussion started: 28 June 2022

Hydrology and Earth System Sciences Discussions

Cammalleri, C., Anderson, M. C., Gao, F., Hain, C. R. and Kustas, W. P.: A data fusion approach for mapping daily evapotranspiration at field scale, Water Resour. Res., 49(8), 4672–4686, doi:10.1002/wrcr.20349, 2013.

Cammalleri, C., Anderson, M. C., Gao, F., Hain, C. R. and Kustas, W. P.: Mapping daily evapotranspiration at field scales over rainfed and irrigated agricultural areas using remote sensing data fusion, Agric. For. Meteorol., 186, 1–11, doi:10.1016/j.agrformet.2013.11.001, 2014.

Chen, F., Crow, W. T., Starks, P. J. and Moriasi, D. N.: Improving hydrologic predictions of a catchment model via assimilation of surface soil moisture, Adv. Water Resour., 34(4), 526–536, doi:10.1016/j.advwatres.2011.01.011, 2011.

Chen, Y., Marek, G. W., Marek, T. H., Brauer, D. K. and Srinivasan, R.: Assessing the efficacy of the SWAT auto-irrigation function to simulate irrigation, evapotranspiration, and crop response to management strategies of the texas high plains, Water (Switzerland), 9(7), 509, doi:10.3390/w9070509, 2017.

Ding, J. and Zhu, Q.: The accuracy of multisource evapotranspiration products and their applicability in streamflow simulation over a large catchment of Southern China, J. Hydrol. Reg. Stud., 41(April), 101092, doi:10.1016/j.ejrh.2022.101092, 2022.

Dosdogru, F., Kalin, L., Wang, R. and Yen, H.: Potential impacts of land use/cover and climate changes on ecologically relevant flows, J. Hydrol., 584, 124654, doi:10.1016/j.jhydrol.2020.124654, 2020.

Duriancik, L. F., Bucks, D., Dobrowolski, J. P., Drewes, T., Eckles, S. D., Jolley, L., Kellogg, R. L., Lund, D., Makuch, J. R., O'Neill, M. P., Rewa, C. A., Walbridge, M. R., Parry, R. and Weltz,

M. A.: The first five years of the: Conservation effects assessment project, J. Soil Water Conserv., 63(6), 185A-188A, doi:10.2489/jswC.63.6.185A, 2008.

Fisher, T. R., Jordan, T. E., Staver, K. W., Gustafson, A. B., Koskelo, A. I., Fox, R. J., Sutton, A. J., Kana, T., Beckert, K. A., Stone, J. P., McCarty, G. and Lang, M.: The choptank basin in transition: Intensifying agriculture, slow urbanization, and estuarine eutrophication, in Coastal Lagoons: Critical Habitats of Environmental Change., 2010.

Gao, F., Anderson, M., Daughtry, C., Karnieli, A., Hively, D. and Kustas, W.: A within-season approach for detecting early growth stages in corn and soybean using high temporal and spatial resolution imagery, Remote Sens. Environ., 242, 111752, doi:10.1016/j.rse.2020.111752, 2020.

Gassman, P. W., Sadeghi, A. M. and Srinivasan, R.: Applications of the SWAT Model Special Section: Overview and Insights, J. Environ. Qual., 43(1), 1–8, doi:10.2134/jeq2013.11.0466, 2014.

Gigante, V., Iacobellis, V., Manfreda, S., Milella, P. and Portoghese, I.: Influences of leaf area index estimations on water balance modeling in a mediterranean semi-arid basin, Nat. Hazards Earth Syst. Sci., 9(3), 979–991, doi:10.5194/nhess-9-979-2009, 2009.

Green, H. W. and Ampt, G. A.: Studies on soil physics: Flow of air and water through soils, J. Aric. Sci., 4, 11–24, 1911.

Ha, L. T., Bastiaanssen, W. G. M., van Griensven, A., van Dijk, A. I. J. M. and Senay, G. B.: Calibration of spatially distributed hydrological processes and model parameters in SWAT using remote sensing data and an auto-calibration procedure: A case study in a Vietnamese river basin, Water (Switzerland), 10(2), 212, doi:10.3390/w10020212, 2018.

https://doi.org/10.5194/hess-2022-187
Preprint. Discussion started: 28 June 2022

Hydrology and Earth System Sciences
Discussions

Haas, H., Kalin, L. and Srivastava, P.: Improved forest dynamics leads to better hydrological predictions in watershed modeling, Sci. Total Environ., 821, 153180, doi:10.1016/j.scitotenv.2022.153180, 2022.

Hain, C. R., Crow, W. T., Anderson, M. C. and Tugrul Yilmaz, M.: Diagnosing neglected soil moisture source-sink processes via a thermal infrared-based two-source energy balance model, J. Hydrometeorol., 16, 1070–1086, doi:10.1175/JHM-D-14-0017.1, 2015.

Hallouin, T.: HydroEval: Streamflow Simulations Evaluator (Version 0.0. 3), 2020.

Hargreaves, G. L., Hargreaves, G. H. and Riley, J. P.: Agricultural Benefits for Senegal River Basin, J. Irrig. Drain. Eng., 111(2), 113–124, doi:10.1061/(asce)0733-9437(1985)111:2(113), 1985.

Herman, M. R., Nejadhashemi, A. P., Abouali, M., Hernandez-Suarez, J. S., Daneshvar, F., Zhang, Z., Anderson, M. C., Sadeghi, A. M., Hain, C. R. and Sharifi, A.: Evaluating the role of evapotranspiration remote sensing data in improving hydrological modeling predictability, J. Hydrol., 556, 39–49, doi:10.1016/j.jhydrol.2017.11.009, 2018.

Hively, W. D., Lee, S., Sadeghi, A. M., McCarty, G. W., Lamb, B. T., Soroka, A., Keppler, J., Yeo, I. Y. and Moglen, G. E.: Estimating the effect of winter cover crops on nitrogen leaching using cost-share enrollment data, satellite remote sensing, and Soil and Water Assessment Tool (SWAT) modeling, J. Soil Water Conserv., 75(3), 362–375, doi:10.2489/JSWC.75.3.362, 2020.

Jiang, D. and Wang, K.: The role of satellite-based remote sensing in improving simulated streamflow: A review, Water (Switzerland), 1615, doi:10.3390/w11081615, 2019.

Julich, S., Breuer, L. and Frede, H. G.: Integrating heterogeneous landscape characteristics into watershed scale modelling, Adv. Geosci., 31, 31–38, doi:10.5194/adgeo-31-31-2012, 2012.

Lee, S., Yeo, I.-Y., Sadeghi, A. M., McCarty, G. W., Hively, W. D. and Lang, M. W.: Impacts of watershed characteristics and crop rotations on winter cover crop nitrate-nitrogen uptake capacity within agricultural watersheds in the Chesapeake Bay region, PLoS One, 11(6), e0157637, doi:10.1371/journal.pone.0157637, 2016.

Lee, S., Yeo, I.-Y., Lang, M. W., McCarty, G. W., Sadeghi, A. M., Sharifi, A., Jin, H. and Liu, Y.: Improving the catchment scale wetland modeling using remotely sensed data, Environ. Model. Softw., 122, 104069, doi:10.1016/j.envsoft.2017.11.001, 2019.

Lee, S., Qi, J., McCarty, G. W., Anderson, M., Yang, Y., Zhang, X., Moglen, G. E., Kwak, D., Kim, H., Lakshmi, V. and Kim, S.: Combined use of crop yield statistics and remotely sensed products for enhanced simulations of evapotranspiration within an agricultural watershed, Agric. Water Manag., 264(January), 107503, doi:10.1016/j.agwat.2022.107503, 2022.

McCarty, G. W., McConnell, L. L., Hapeman, C. J., Sadeghi, A., Graff, C., Hively, W. D., Lang, M. W., Fisher, T. R., Jordan, T., Rice, C. P., Codling, E. E., Whitall, D., Lynn, A., Keppler, J. and Fogel, M. L.: Water quality and conservation practice effects in the Choptank River watershed, J. Soil Water Conserv., 63(6), 461–474, doi:10.2489/jswc.63.6.461, 2008.

McKay, M. D., Beckman, R. J. and Conover, W. J.: A comparison of three methods for selecting values of input variables in the analysis of output from a computer code, Technometrics, 21(2), 239–245, doi:10.1080/00401706.2000.10485979, 2000.

Monteith, J. L.: Evaporation and environment., in Symposia of the Society for Experimental Biology, pp. 205–234, Cambridge Univ. Press, London., 1965.

https://doi.org/10.5194/hess-2022-187
Preprint. Discussion started: 28 June 2022

Moriasi, D. N., Arnold, J. G., Van Liew, M. W., Bingner, R. L., Harmel, R. D. and Veith, T. L.: Model Evaluation Guidelines for Systematic Quantification of Accuracy in Watershed Simulations, Trans. ASABE, 50(3), 885–900, doi:10.13031/2013.23153, 2007.

Myneni, R. B., Hoffman, S., Knyazikhin, Y., Privette, J. L., Glassy, J., Tian, Y., Wang, Y., Song, X., Zhang, Y., Smith, G. R., Lotsch, A., Friedl, M., Morisette, J. T., Votava, P., Nemani, R. R. and Running, S. W.: Global products of vegetation leaf area and fraction absorbed PAR from year one of MODIS data, Remote Sens. Environ., 83, 214–231, doi:10.1016/S0034-4257(02)00074-3, 2002.

Neitsch, S. ., Arnold, J. ., Kiniry, J. . and Williams, J. .: Soil & Water Assessment Tool Theoretical Documentation Version 2009., 2011.

Norman, J. M., Kustas, W. P. and Humes, K. S.: Source approach for estimating soil and vegetation energy fluxes in observations of directional radiometric surface temperature, Agric. For. Meteorol., 77, 263–293, doi:10.1016/0168-1923(95)02265-Y, 1995.

Parajuli, P. B., Jayakody, P. and Ouyang, Y.: Evaluation of Using Remote Sensing Evapotranspiration Data in SWAT, Water Resour. Manag., 32(3), 985–996, doi:10.1007/s11269-017-1850-z, 2018.

Poméon, T., Diekkrüger, B., Springer, A., Kusche, J. and Eicker, A.: Multi-objective validation of SWAT for sparsely-gaugedWest African river basins - A remote sensing approach, Water (Switzerland), 10(4), 451, doi:10.3390/w10040451, 2018.

Priestley, C. H. B. and Taylor, R. J.: On the Assessment of Surface Heat Flux and Evaporation Using Large-Scale Parameters, Mon. Weather Rev., 100, 81–92, doi:10.1175/1520-0493(1972)100<0081:otaosh>2.3.co;2, 1972.

https://doi.org/10.5194/hess-2022-187
Preprint. Discussion started: 28 June 2022

Qi, J., Wang, Q. and Zhang, X.: On the use of NLDAS2 weather data for hydrologic modeling in the Upper Mississippi River Basin, Water (Switzerland), 11(5), 960, doi:10.3390/w11050960, 2019.

Rajib, A., Evenson, G. R., Golden, H. E. and Lane, C. R.: Hydrologic model predictability improves with spatially explicit calibration using remotely sensed evapotranspiration and biophysical parameters, J. Hydrol., 567, 668–683, doi:10.1016/j.jhydrol.2018.10.024, 2018.

Rajib, A., Kim, I. L., Golden, H. E., Lane, C. R., Kumar, S. V., Yu, Z. and Jeyalakshmi, S.: Watershed modeling with remotely sensed big data: Modis leaf area index improves hydrology and water quality predictions, Remote Sens., 12(13), 2148, doi:10.3390/rs12132148, 2020.

Savitzky, A. and Golay, M. J. E.: Smoothing and Differentiation of Data by Simplified Least Squares Procedures, Anal. Chem., 36(8), 1627–1639, doi:10.1021/ac60214a047, 1964.

Schlesinger, W. H. and Jasechko, S.: Transpiration in the global water cycle, Agric. For. Meteorol., 189(115), 117, doi:10.1016/j.agrformet.2014.01.011, 2014.

Seibert, J. and McDonnell, J. J.: On the dialog between experimentalist and modeler in catchment hydrology: Use of soft data for multicriteria model calibration, Water Resour. Res., 38(11), 1241, doi:10.1029/2001wr000978, 2002.

Sexton, A. M., Sadeghi, A. M., Zhang, X., Srinivasan, R. and Shirmohammadi, A.: Using NEXRAD and rain gauge precipitation data for hydrologic calibration of SWAT in a northeastern watershed, Trans. ASABE, 53(5), 1501–1510, doi:10.13031/2013.34900, 2010.

Sharifi, A., Lang, M. W., McCarty, G. W., Sadeghi, A. M., Lee, S., Yen, H., Rabenhorst, M. C., Jeong, J. and Yeo, I.-Y.: Improving model prediction reliability through enhanced representation of wetland soil processes and constrained model auto calibration – A paired watershed study, J. Hydrol., 541, 1088–1103, doi:10.1016/j.jhydrol.2016.08.022, 2016.

Shirmohammadi, A., Chaubey, I., Harmel, R. D., Bosch, D. D., Muñoz-Carpena, R., Dharmasri, C., Sexton, A. M., Arabi, M., Wolfe, M. L., Frankenberger, J., Graff, C. and Sohrabi, T. M.: Uncertainty in TMDL models, Trans. ASABE, 49(4), 1033–1049, doi:10.13031/2013.21741, 2006.

Stisen, S., Jensen, K. H., Sandholt, I. and Grimes, D. I. F.: A remote sensing driven distributed hydrological model of the Senegal River basin, J. Hydrol., 354(1–4), 131–148, doi:10.1016/j.jhydrol.2008.03.006, 2008.

Strauch, M. and Volk, M.: SWAT plant growth modification for improved modeling of perennial vegetation in the tropics, Ecol. Modell., 269, 98–112, doi:10.1016/j.ecolmodel.2013.08.013, 2013.

Sun, L., Anderson, M. C., Gao, F., Hain, C., Alfieri, J. G., Sharifi, A., McCarty, G. W., Yang, Y., Yang, Y., Kustas, W. P. and McKee, L.: Investigating water use over the Choptank River Watershed using a multisatellite data fusion approach, Water Resour. Res., 53, 5298–5319, doi:10.1002/2017WR020700, 2017.

Ukkola, A. M. and Prentice, I. C.: A worldwide analysis of trends in water-balance evapotranspiration, Hydrol. Earth Syst. Sci., 17, 4177–4187, doi:10.5194/hess-17-4177-2013, 2013.

USDA-SCS: Section 4: Hydrology, in National Engineering Handbook., 1972.

Vaché, K. B. and McDonnell, J. J.: A process-based rejectionist framework for evaluating catchment runoff model structure, Water Resour. Res., 42(2), doi:10.1029/2005WR004247, 2006.

Vervoort, R. W., Miechels, S. F., van Ogtrop, F. F. and Guillaume, J. H. A.: Remotely sensed evapotranspiration to calibrate a lumped conceptual model: Pitfalls and opportunities, J. Hydrol., 519, 3223–3236, doi:10.1016/j.jhydrol.2014.10.034, 2014.

Wambura, F. J., Dietrich, O. and Lischeid, G.: Improving a distributed hydrological model using evapotranspiration-related boundary conditions as additional constraints in a data-scarce river basin, Hydrol. Process., 32(6), 759–775, doi:10.1002/hyp.11453, 2018.

Wang, K., Dickinson, R. E., Wild, M. and Liang, S.: Evidence for decadal variation in global terrestrial evapotranspiration between 1982 and 2002: 1. Model development, J. Geophys. Res. Atmos., 115(D20), doi:10.1029/2009JD013671, 2010.

Winchell, M., Srinivasan, R., Di Luzio, M. and Arnold, J.: ArcSWAT interface for SWAT 2005, User's Guid., 2007.

Wolman, M. G.: Water for Maryland's Future: What We Must Do Today, Baltimore, Md., 2008.

Wu, K. and Xu, Y. J.: Evaluation of the applicability of the SWAT model for coastal watersheds in southeastern Louisiana, J. Am. Water Resour. Assoc., 42(5), 1247–1260, doi:10.1111/j.1752-1688.2006.tb05610.x, 2006.

Xu, X., Li, J. and Tolson, B. A.: Progress in integrating remote sensing data and hydrologic modeling, Prog. Phys. Geogr., 38(4), 464–498, doi:10.1177/0309133314536583, 2014.

https://doi.org/10.5194/hess-2022-187
Preprint. Discussion started: 28 June 2022

Hydrology and Earth System Sciences
Discussions

Yan, H., Wang, S. Q., Billesbach, D., Oechel, W., Zhang, J. H., Meyers, T., Martin, T. A., Matamala, R., Baldocchi, D., Bohrer, G., Dragoni, D. and Scott, R.: Global estimation of evapotranspiration using a leaf area index-based surface energy and water balance model, Remote Sens. Environ., 124, 581–595, doi:10.1016/j.rse.2012.06.004, 2012.

Yang, Q. and Zhang, X.: Improving SWAT for simulating water and carbon fluxes of forest ecosystems, Sci. Total Environ., 569–570, 1478–1488, doi:10.1016/j.scitotenv.2016.06.238, 2016.

Yen, H., Wang, X., Fontane, D. G., Harmel, R. D. and Arabi, M.: A framework for propagation of uncertainty contributed by parameterization, input data, model structure, and calibration/validation data in watershed modeling, Environ. Model. Softw., 43(5), 1601–1613, doi:10.1016/j.envsoft.2014.01.004, 2014a.

Yen, H., Bailey, R. T., Arabi, M., Ahmadi, M., White, M. J. and Arnold, J. G.: The Role of Interior Watershed Processes in Improving Parameter Estimation and Performance of Watershed Models, J. Environ. Qual., 43(5), 1601–1613, doi:10.2134/jeq2013.03.0110, 2014b.

Yen, H., White, M. J., Ascough, J. C., Smith, D. R. and Arnold, J. G.: Augmenting Watershed Model Calibration with Incorporation of Ancillary Data Sources and Qualitative Soft Data Sources, J. Am. Water Resour. Assoc., 52(3), 788–798, doi:10.1111/1752-1688.12428, 2016.

Yeo, I.-Y., Lee, S., Sadeghi, A. M., Beeson, P. C., Hively, W. D., McCarty, G. W. and Lang, M. W.: Assessing winter cover crop nutrient uptake efficiency using a water quality simulation model, Hydrol. Earth Syst. Sci., 18(12), 5239–5253, doi:10.5194/hess-18-5239-2014, 2014.

Yeo, I.-Y., Lee, S., Lang, M. W., Yetemen, O., McCarty, G. W., Sadeghi, A. M. and Evenson, G.: Mapping landscape-level hydrological connectivity of headwater wetlands to downstream

https://doi.org/10.5194/hess-2022-187
Preprint. Discussion started: 28 June 2022

waters: A catchment modeling approach - Part 2, Sci. Total Environ., 653, 1557 – 1570, doi:10.1016/j.scitotenv.2018.11.237, 2019.

Zhao, F., Wu, Y., Wang, L., Liu, S., Wei, X., Xiao, J., Qiu, L. and Sun, P.: Multi-environmental impacts of biofuel production in the U.S. Corn Belt: A coupled hydro-biogeochemical modeling approach, J. Clean. Prod., 251, 119561, doi:10.1016/j.jclepro.2019.119561, 2020.